Brain, Behavior, & Immunity - Health 53 (2026) 101207

Contents lists available at ScienceDirect

Brain, Behavior, & Immunity - Health

journal homepage: www.editorialmanager.com/bbih/default.aspx

Multi-omic analysis reveals brain–blood concordance and persistent neuroimmune reprogramming with stress and toxicant exposure in a mouse model of Gulf War Illness

A. Sasaki [a], K.A. Kelly [b], L.T. Michalovicz [b], D.G. Ashbrook [a,c], S. Wijenayake [a,1], J.P. O'Callaghan [b], P.O. McGowan [a,d,e,*]

[a] Biological Sciences, University of Toronto, Toronto, ON, Canada
[b] Centers for Disease Control and Prevention, National Institute for Occupational Safety and Health, Morgantown, WV, USA
[c] Department of Genetics, Genomics and Informatics, The University of Tennessee Health Science Center, Memphis, TN, USA
[d] Department of Cell and Systems Biology, University of Toronto, Toronto, ON, Canada
[e] Department of Physiology, University of Toronto, Toronto, ON, Canada

ARTICLE INFO

Keywords:
Gulf War Illness
Neuroinflammation
DNA methylation modifications
Hippocampus
Stress and toxicant exposure
Transcriptomics
Epigenetic signatures

ABSTRACT

Gulf War Illness (GWI) is a chronic neuroimmune condition affecting veterans of the 1990–91 Gulf War. Current treatments primarily target symptom relief, and the biological mechanisms underlying GWI remain poorly understood. Using a validated mouse model of Gulf War Illness (GWI) combining corticosterone (CORT) and diisopropyl fluorophosphate (DFP) exposure to induce stress- and toxicant-related neuroimmune priming, we examined how prior exposure alters molecular responses to a subsequent immune challenge. Male mice were exposed to CORT and DFP with repeated intermittent CORT, followed by lipopolysaccharide (LPS) or saline to assess transcriptional and epigenetic changes in brain and blood. We analysed transcript abundance, chromatin accessibility, and DNA methylation in the hippocampus, frontal cortex, and blood at 6 h, 12 h and 24hrs after LPS challenge (3-4 mice per group). We identified widespread transcriptional changes and dynamic chromatin accessibility following LPS exposure, with DNA methylation modifications that persisted in the hippocampus and blood. Thirty-three genes, including *Stat3*, *Plpp3*, *Cdkn1a*, and *Fgfr2*, were differentially expressed and methylated in both hippocampus and blood across all time points. These genes clustered in immune- and glial-related pathways. Transcription factor analysis revealed enrichment of NF-κB, CREB1, EGR1, JUN, and MYC binding motifs in regions with differential methylation. Our findings identify novel candidate biomarkers in peripheral blood that reflect brain molecular changes, providing a new framework for elucidating the long-term epigenetic impacts of stress and toxicant exposure in GWI.

1. Introduction

Gulf War Illness (GWI) is a disorder characterized by a multitude of symptoms and neuroimmune dysfunction, bearing similarities to sickness behaviour (Dantzer et al., 2008; O'Callaghan et al., 2015). GWI affects nearly one-third of veterans from the 1990-91 Gulf War, presenting a complex clinical picture that includes fatigue, musculoskeletal pain, cognitive dysfunction, chemical sensitivities, memory loss, and sleep disturbances (Ashbrook et al., 2018; Koo et al., 2017; Locker et al., 2017; O'Callaghan et al., 2015; White et al., 2016). Despite extensive research, current treatment approaches for GWI largely focus on managing symptoms rather than addressing underlying causes of the illness (Michalovicz et al., 2021).

GWI shares stress-linked neuroimmune features, most notably glial/microglial priming with exaggerated cytokine signalling and overlapping cognitive/affective symptoms such as memory problems, fatigue, and mood disturbance, with other stress-related illnesses such as PTSD (e.g. (Dantzer et al., 2008; Passos et al., 2015),). However, stratified analyses in veterans indicate that PTSD is not a primary driver of the clinical presentation of GWI (Sultana et al., 2024), and both clinical and pre-clinical studies implicate exposure to nerve agents in its aetiology (Haley et al., 2022; O'Callaghan et al., 2015). During the Gulf War,

* Corresponding author. Department of Biological Sciences, University of Toronto, 1265 Military Trail, Toronto, ON, M1C 1A4, Canada.
E-mail address: patrick.mcgowan@utoronto.ca (P.O. McGowan).
[1] Present address: Department of Biology, The University of Winnipeg, Winnipeg, MB, Canada.

https://doi.org/10.1016/j.bbih.2026.101207
Received 11 November 2025; Received in revised form 9 February 2026; Accepted 2 March 2026
Available online 11 March 2026
2666-3546/© 2026 The Authors. Published by Elsevier Inc. This is an open access article under the CC BY-NC-ND license (http://creativecommons.org/licenses/by-nc-nd/4.0/).

military personnel were exposed to various acetylcholinesterase (AChE) inhibitors, including pyridostigmine bromide (PB), sarin, soman, and organophosphate pesticides, which were used to prevent pest-borne diseases (White et al., 2016). Exposure to the extreme stress of warfare is proposed to amplify the effect of neurotoxicants on the development of GWI through complex neuroimmune mechanisms. Within this framework, the stress associated with GWI is not exclusively psychological stress but includes high physiological stress resulting from environmental exposures such as excessive heat, exercise, and dehydration.

Our research uses a preclinical mouse model to explore the effects of exposure to corticosterone (CORT), a glucocorticoid stress hormone used as a shared downstream mediator of high stress, and diisopropyl fluorophosphate (DFP), a sarin surrogate. Prior publications from this model have already characterized baseline differences between naïve and CORT + DFP animals. An acute "in theatre" model replicates the immediate and short-term exposure conditions experienced by solders while deployed in a combat zone, with exposure to CORT given immediately prior to DFP (Koo et al., 2017; Locker et al., 2017; O'Callaghan et al., 2015). Our recent study using this acute model demonstrated that these exposures lead to epigenetic modifications and genome-wide changes in transcript abundance in the brain (Ashbrook et al., 2018). Long-term models indicate that repeated, intermittent CORT delivery over a period of weeks following the "in theater" model exacerbates the neuroinflammatory response to subsequent LPS challenge, suggesting a persistent priming of the neuroimmune system (Cheng et al., 2024; Michalovicz et al., 2021). This long-term model extends beyond the acute phase to mimic the chronic condition of GWI that veterans experience long after their deployment.

The primary aim of the present study was to determine how prior exposure to corticosterone and diisopropyl fluorophosphate (CORT + DFP) alters molecular responses in brain and blood to a subsequent immune challenge with lipopolysaccharide (LPS). We examined transcriptomic and epigenomic signatures across hippocampus (HPC) and cortex (CTX), along with epigenomic signatures in peripheral blood, to test the following hypotheses: (i) CORT + DFP potentiates and reprograms neuroimmune responses to LPS in brain; (ii) a subset of these changes would be reflected in blood, indicating cross-tissue concordance; and (iii) the primed response would occur with distinct temporal dynamics (6–24 h) consistent with stress-toxicant sensitisation. We further hypothesised that DNA-methylation signatures would align with expression changes in pathways involved in innate immune signalling and glial function, supporting a persistent neuroimmune reprogramming. Region selection was guided by prior CORT + DFP GWI models showing robust, time-dependent neuroinflammatory responses in HPC and CTX that are amplified by glucocorticoid priming, with related microstructural alterations on diffusion imaging in the same paradigm (Koo et al., 2017; Locker et al., 2017; O'Callaghan et al., 2015).

2. Materials and methods

2.1. Animals and subject numbers

Adult male C57Bl/6J mice (8-12 weeks old, ~30g) were obtained from Jackson Laboratory (Bar Harbor, ME, USA). All procedures adhered to protocols approved by the US Centers for Disease Control and Prevention-Morgantown Institutional Animal Care and Use Committee and the US Army Medical Research and Materiel Command Animal Care and Use Review Office. The animal facility was accredited by AAALAC International. Upon arrival, the mice were housed individually in a colony room with controlled temperature (21 ± 1 °C) and humidity (50 ± 10%), maintained under filtered positive-pressure ventilation. The light-dark cycle was set to 12 h each, starting at 06:00 h. The mice had continuous access to Teklad 7913 irradiated NIH-31 modified 6% rodent chow and water. Mice were assigned to four exposure/time-point groups followed by an acute immune challenge: (1) CORT + DFP + Saline (baseline control at 6 h), (2) CORT + DFP + LPS (6 h), (3) CORT + DFP + LPS (12 h), and (4) CORT + DFP + LPS (24 h) (also see §2.2). Across assays, a total of 31 animals were analysed. The CORT + DFP + Saline group at +6 h served as the baseline comparator for 1-vs-1 contrasts at each LPS time point (i.e., 6 h, 12 h, 24 h) (also see §2.8). At study start, animals were randomised to exposure/time-point groups using simple randomisation. Sample processing order for molecular assays was also randomised. Library preparation and computational analyses were conducted with group identifiers masked until primary QC and alignment metrics were completed. Separate cohorts were used for qPCR, RNA-seq, RRBS, and ATAC-seq. Samples sizes are reported at first mention in the relevant Methods section and again in the relevant figure legends (qPCR §2.4/Fig. 2; RNA-seq §2.4/Fig. 3; ATAC-seq §2.6/Fig. 5; RRBS §2.7/Fig. 6), with QC-related exclusions detailed in those sections.

2.2. Dosing preparations

The dosing paradigm is presented in Fig. 1. To replicate the long-term GWI model developed in mice (Michalovicz et al., 2021), adult male C57BL/6J mice were given CORT in the drinking water (200 mg/L in 0.6% EtOH; Steraloids, Newport, RI, USA) for 7 days. As described previously, this regimen of CORT was selected to induce circulating levels of stress hormone like those induced by repeated behavioural stress paradigms, also produce significant immunosuppression (Locker et al., 2017; Michalovicz et al., 2021). On day 8, mice were given a single intraperitoneal injection of a sarin surrogate, DFP (4 mg/kg, MilliporeSigma, St. Louis, MO, USA). This is then followed by periodic administration of CORT for 7 days every other week to a total of 5 weeks, a single subcutaneous injection of LPS (0.5 mg/kg, MilliporeSigma) or saline on the final day.

For the four exposure groups, the dosing regimen was as follows: (1) CORT + DFP + Saline (control): CORT for 1 week, DFP injection followed by 4 weeks of intermittent CORT, then sacrificed at 6hrs post saline injection on the final day; (2) CORT + DFP + LPS (6hrs): CORT for 1 week, DFP injection followed by 4 weeks of intermittent CORT, then sacrificed at 6hrs post LPS injection on the final day; (3) CORT + DFP + LPS (12hrs): CORT for 1 week, DFP injection followed by 4 weeks of intermittent CORT, then sacrificed at 12hrs post LPS injection on the final day; and (4) CORT + DFP + LPS (24hrs): CORT for 1 week, DFP injection followed by 4 weeks of intermittent CORT, then sacrificed at 24hrs post LPS injection on the final day. In all subsequent analyses, the *CORT + DFP + Saline* group served as the control, representing the chronically primed state without acute immune activation. This design follows the established long-term GWI model (Michalovicz et al., 2021) to specifically examine how an immune challenge alters molecular responses within that primed neuroimmune context. While naïve saline-only controls were not included, the present design controls for CORT + DFP exposure history across all groups, isolating the LPS-induced component of the primed response.

2.3. Brain dissection and tissue preparation

Mice were euthanized by swift decapitation and both the brains and trunk blood were collected. The entire HPC and the CTX, which includes

the anterior section of the cortex (Franklin and Paxinos, 2013; O'Callaghan et al., 2015) were dissected manually on a thermoelectric cooling platform (Model TCP-2; Aldrich Chemical Co., Milwaukee, WI, USA). Brain and whole blood samples were promptly frozen at −80 °C.

2.4. Differential gene expression and RNA sequencing

Total RNA was extracted from the HPC and CTX using the E.Z.N.A. RNA/DNA Isolation Kit from Omega Biotek (Norcross, Georgia, USA) and reverse transcribed to cDNA as previously described (Ashbrook et al., 2018; Kelly et al., 2018; Locker et al., 2017).

Gene expression analysis was performed using an AB7500 Real-Time PCR machine with Taqman chemistry (Thermo Fisher Scientific, Waltham, MA, USA) for a subset of inflammatory genes identified in our previous studies to be differentially expressed (*Tnfa, Il-6, Ccl2, Il-1b*, and *Osm*) (n = 4 per treatment/time point). For these analyses, relative expression was determined by the comparative Ct (ΔΔCt) method with Gapdh as the reference and CORT–DFP as the control group (Livak and Schmittgen, 2001). Because fold-change is ratio-scale, we analysed $\log_2$(fold-change) (equivalent to −ΔΔCt) to meet ANOVA assumptions, and report back-transformed fold-changes (FC = 2estimate) with 95% CIs. For each gene, we fit a two-way ANOVA with fixed factors brain region (HPC, CTX) and timepoint (Control, 6 h, 12 h, 24 h). Planned comparisons of each LPS timepoint with Control were performed within each brain region using emmeans; *p*-values were adjusted by Benjamini–Hochberg FDR (Benjamini and Hochberg, 1995) across all timepoint-vs-control tests (genes × brain region). Simple HPC vs CTX contrasts were tested at each timepoint with FDR control. Assumptions were checked via residual diagnostics and Levene's test; estimated marginal means (EMMs) with 95% CIs are reported on the fold-change scale.

For RNA-seq, poly(A)-selected, stranded mRNA libraries were prepared with the *Illumina TruSeq Stranded mRNA Library Prep Kit* following the manufacturer's protocol. Whole-genome mRNA sequencing was performed on the Illumina NovaSeq 6000 at the Donnelly Sequencing Centre (Toronto, ON, Canada) using paired-end reads with a length of 150 bp. Due to poor sample quality, one control HPC sample was excluded from analysis.

Fastq files were processed to remove adaptor sequences and low-quality reads (q < 30) using TrimGalore version 0.4.1 (Krueger and Andrews, 2011), which relies on Cutadapt (version 1.15) (Martin, 2011). The quality of pre-processed reads was assessed with FastQC (Krueger and Andrews, 2011). Trimmed reads were aligned using STAR (Dobin et al., 2013) (version 2.6.0a) in a two-pass mode. The reference genome GENCODE GRCm38.p4 (mm10) and associated annotations were retrieved from the GENCODE database (Mudge and Harrow, 2015). The CTX samples had an average of 23,391,972 reads per sample, with 88% of reads successfully mapped. HPC samples had an average of 26,157,954 reads per sample, with 89% of reads mapped.

The resulting BAM files were processed using GenomicAlignments and DESeq2 (version 1.10.1) R packages following the standard DESeq2 workflow (Love et al., 2014). In short, DESeq2 applies a generalized linear model for each gene, treating read counts as following a negative binomial distribution. Dispersion estimates are adjusted using an empirical Bayes method, and the Wald test is employed for statistical significance testing, with multiple testing corrections applied using the Benjamini-Hochberg method (Benjamini and Hochberg, 1995).

For power analysis of the RNA-seq data, we performed a design-based analysis using the negative binomial framework implemented in DESeq2, which models read counts as a function of mean expression and a dispersion parameter. The square root of dispersion is the biological coefficient of variation (BCV), which quantifies biological variability across replicates. Our empirical dispersion fits yielded median BCVs of 0.30 (IQR 0.07–1.45) in HPC and 0.30 (IQR 0.10–1.47) in CTX, consistent with the expected range for inbred C57BL/6 mice of the same sex and age (BCV ≈ 0.20–0.30; Law et al., 2014; Cheng et al., 2024). Using these values, we calculated minimum detectable effect sizes (MDES) at 80% power and FDR 5%. At moderate expression levels, n = 3/group corresponds to MDES ≈ log2FC 1.27 (~2.4-fold) in HPC and log2FC 1.24 (~2.4-fold) in CTX, while n = 4/group corresponds to MDES ≈ log2FC 1.10 (~2.1-fold) in HPC and log2FC 1.07 (~2.1-fold) in CTX. These analyses demonstrate that our design is well powered to detect moderate-to-large expression changes (Love et al., 2014).

2.5. Cell proportion estimation

The DeconRNASeq package from R Bioconductor was used to estimate the relative proportions of different cell types in RNA-seq samples (Gong and Szustakowski, 2013). To establish a reference for cell type-specific gene expression, data enriched for central nervous system (CNS) cell types was obtained from the Gene Expression Omnibus (GEO) Series GSE52564, which contains gene expression profiles from the *Mus musculus* cerebral cortex.

RNA-seq data underwent preprocessing steps including trimming, alignment, and quantification of gene expression. Expression profiles were determined for six distinct cell types—astrocytes, neurons, oligodendrocyte precursor cells (OPCs), myelinating oligodendrocytes (MOs), microglia, and endothelial cells—by identifying genes that showed at least a five-fold higher expression in one cell type relative to the others.

Based on these expression signatures, DeconRNASeq was applied to estimate the proportions of astrocytes, neurons, OPCs, MOs, microglia, and endothelial cells in 15 cortex samples and 15 HPC samples. This package utilizes a linear model that aggregates pure tissue or cell-type-specific read counts, weighted according to each cell type's proportion. The algorithm solves a non-negative least-squares problem through quadratic programming, enabling the detection of cell types comprising as little as ~2% of the total sample population.

Estimated cell-type proportions were analysed separately for cortex (CTX) and hippocampus (HPC). Because proportions are compositional data (they are bounded between 0 and 1 and always sum to one), we used log-ratio transformations for these statistical tests. Specifically, we applied an isometric log-ratio (ILR) transform to obtain independent coordinates and tested for overall time effects (0, 6, 12, 24 h) using MANOVA. To examine specific cell types, we used centred log-ratio (CLR) ANOVA with Benjamini–Hochberg false discovery rate (FDR) control (q = 0.05). As a robustness check, we also fit Dirichlet regression models (composition ~ time) and compared full vs reduced models (where time is not included) by likelihood-ratio tests.

2.6. ATAC sequencing and differential peak analyses

ATAC-seq libraries for the HPC and CTX were generated from frozen tissue samples (20–30 mg) using the OMNI-ATAC Seq protocol (Corces et al., 2017). Sequencing was performed on a NovaSeq6000 at the Princess Margaret Genomics Centre (Toronto, ON, Canada) using

paired-end reads with a length of 50 bp. One control subject was excluded due to low numbers of reads.

Initial data analysis was conducted by the Centre for the Analysis of Genome Evolution & Function (CAGEF) at the University of Toronto (Toronto, Ontario, Canada). Raw sequencing reads were processed using Trim Galore (v0.6.7) alongside FASTQC (v0.11.9) for adapter removal and quality control. The average read count exceeded 57 million per sample. Trimmed reads were aligned to the mouse reference genome (mm10) using Bowtie2 (v2.4.4) with default settings, achieving a post-alignment mapping rate of 98–99% across all samples.

ATAC-seq peaks were identified using MACS2 (v2.2.7.1) (Zhang et al., 2008), with most peaks measuring 1 KB or less. Differential peak analysis was carried out using the Bioconductor package csaw (Lun and Smyth, 2016), which detects differentially accessible regions between conditions. This method employs a window-based approach to enhance both sensitivity and specificity in identifying differential binding events.

For power analysis of the ATAC-seq data, we analysed peak counts using the same count-based models (DESeq2/edgeR) as for RNA-seq. The ENCODE consortium guidelines specify a minimum of two biological replicates, with three or more recommended for robust detection of differential accessibility. Our groups of n = 3–4 therefore meet or exceed these standards and are consistent with current best practice (Corces et al., 2017).

2.7. RRBS and differential methylation

HPC and CTX DNA were extracted using E.Z.N.A. RNA/DNA Isolation kit by Omega Biotek (Norcross, Georgia) from the same samples as above for RNA-seq, and blood DNA was extracted using the QIAampDNA blood kit (Qiagen). RRBS libraries were then generated from high-quality dsDNA (100 ng with DNA Integrity Numbers >7) for each subject using the Ovation NuGen RRBS Kit (San Carlos, CA, USA) and EpiTect Fast DNA Bisulfite Conversion kit (Qiagen) following the manufacturer's protocols. RRBS libraries were sequenced by Donnelly Sequencing Centre (Toronto, ON, Canada) on a NextSeq500 following the manufacturer's protocols for single end reads of 75 bp read length. One sample from 12h and 24h conditions were removed for the blood samples and one sample from Control and one sample from the 12h condition was removed for the HPC samples due to low numbers of reads.

RRBS FASTQ files were trimmed to remove adaptors and low-quality bases (Phred score <30) using TrimGalore (v0.4.1) (Krueger, 2015), which wraps around Cutadapt (v2.8) (Martin, 2011). Trimmed reads were then aligned to the GRCm38 (mm10) mouse reference genome using Bismark (v0.16.0) (Krueger and Andrews, 2011), which is built on Bowtie2 (v2.3.5.1) (Langmead and Salzberg, 2012). The average reads per sample was 31,862,559 with 62% mapping efficiency for the frontal cotex, and for the HPC, the average reads per sample was 27,989,562, 62% mapping efficiency. For the blood samples, the average reads per sample was 31,862,560 with 62% mapping efficiency. The resulting BAM files were analysed with methylKit (1.26.0) (Akalin et al., 2012), using the recommended methods. The bisulfite conversion rate exceeded 99.1% for all samples. Methylation levels for each cytosine site were estimated as probabilities based on the ratio of methylated to total reads at each locus. Differential methylation was calculated using logistic regression.

RRBS power is driven by per-site read depth and CpG-level variance, and prospective Minimum Detectable Effect Size (MDES) frameworks are not yet well established. We therefore used conservative criteria to ensure robust calls for differentially methylated cytosines (DMCs): ≥10 × coverage in every sample, ≥5% between-group methylation difference, and FDR-adjusted $p < 0.05$ from methylKit logistic regression, consistent with published guidance (Akalin et al., 2012; Dolzhenko and Smith, 2014; Park and Wu, 2016).

2.8. Identifying genes unique to LPS exposure at each time point

A series of 1v1 comparisons were made to conservatively estimate which genes were differentially expressed (RNA-seq), had differential open chromatin peaks (ATAC-seq) or were differentially methylated (RRBS). To identify changes attributable to LPS exposure, all comparisons were made relative to the *CORT + DFP + Saline* group, which functioned as the baseline control condition.

1. CORT + DFP + Saline vs CORT + DFP + LPS (6hrs)
2. CORT + DFP + Saline vs CORT + DFP + LPS (12hrs)
3. CORT + DFP + Saline vs CORT + DFP + LPS (24hrs)

2.9. Gene pathway enrichment analysis

Gene pathways associated with the top 100 differentially expressed or methylated genes were evaluated using the biological process category in Gene Ontology (GO). The enrichment analysis was performed using Molecular Signatures Database (MSigDB) (Subramanian et al., 2005) with significant enrichment tested with a hypergeometric framework and Benjamini–Hochberg FDR control (significant at FDR <0.05). The background set was the union of genes observed in the relevant analysis (i.e., all genes passing preprocessing for that dataset).

For DNA methylation gene sets, we focused on sustained gene-level changes across time. For each time point (6hrs, 12hrs, 24hrs), CpGs with FDR <0.05 were kept. Unique genes appearing among significant CpGs at all three time points formed the DNA methylation gene set. For each gene we took the smallest q-value observed across CpGs and times and ranked genes by this value. Gene Ontology enrichment was performed with goseq (mm10 *knownGene* (Young et al., 2010);), which adjusts for gene-length bias, using the union of all observed genes as the background and controlling FDR with Benjamini–Hochberg.

2.10. Transcription factor binding site analysis using MEME suite

We identified genes that exhibited differential expression, ATAC-seq peak enrichment, and DNA methylation at any point during the experimental timeline. This multi-omic approach was designed to enable comprehensive selection of candidate genes for subsequent analysis. For DNA methylation analysis, we extracted DMCs based on the gene list generated from this differential analysis. To ensure thorough coverage, we analysed sequences ±50 base pairs (bp) upstream and downstream of each DMC. This extension facilitated the capture of potential regulatory regions adjacent to the DMCs. To mitigate potential biases introduced by overlapping DNA sequences, we combined any overlapping extended regions. This step was implemented to maintain the integrity and independence of the sequences used in downstream analyses.

Next, we used the Find Individual Motif Occurrences (FIMO) tool, part of the MEME Suite, to scan the prepared DNA sequences for potential transcription factor binding sites.

(Bailey et al., 2015). FIMO was run against the mouse genome (mm10) using the JASPAR CORE vertebrate non-redundant

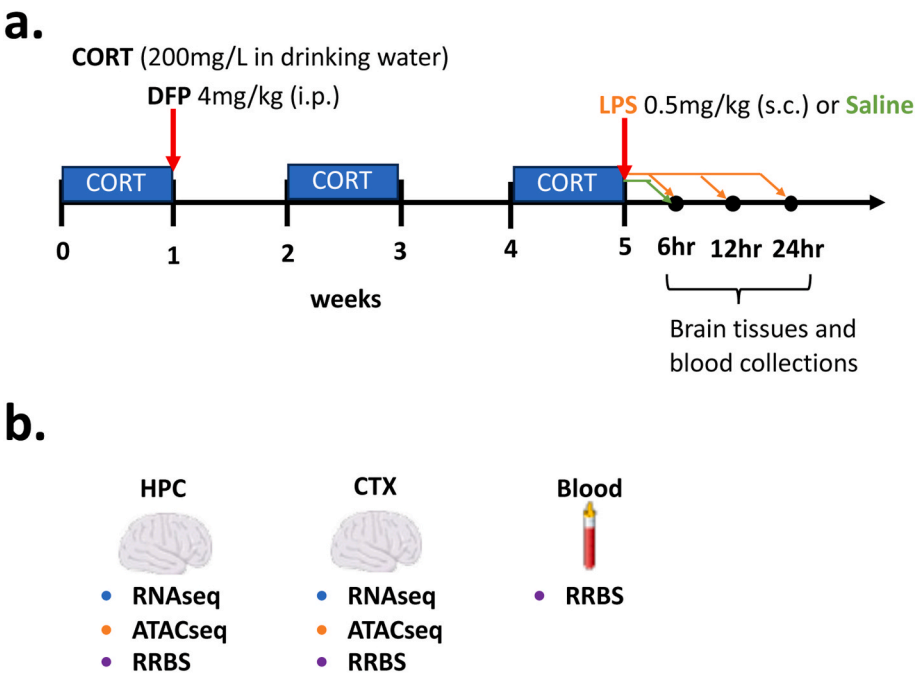

Fig. 1. Study design and multi-omics sampling. **a.** In this long-term exposure model, male mice (n = 3-4/treatment/time point) are initially exposed to CORT (200 mg/L) in the drinking water for 7 days followed by a single, acute injection of DFP (4 mg/kg, i.p.). This is then followed by periodic administration of CORT for 7 days every other week to a total of 5 weeks, with LPS (0.5 mg/kg, s.c.) or saline administered on the final day prior to euthanasia at 6hr, 12h or 24h post-injection. **b.** Tissue profiled and assays performed: hippocampus (HPC) and cortex (CTX) for RNA-seq, ATAC-seq, and RRBS; blood for RRBS. Brain images provided by Servier Medical Art (https://smart.servier.com), licensed under CC BY 4.0 (https://creativecommons.org/licenses/by/4.0/). Blood in tube image adapted from FreeSVG (SVG ID, 202659, Public Domain/CCO).

transcription factor database (Fornes et al., 2020). This database provides a comprehensive collection of experimentally verified transcription factor binding motifs for the identification of binding sites.

We then performed two complementary motif scans using the MEME Suite with the ATAC-seq data. First, to examine overlap with DMCs, Differentially Accessible Regions (DARs) were called from ATAC-seq using MACS2 followed by differential analysis with csaw. As DAR coordinates were originally in mm9, they were converted to mm10 with UCSC liftOver (≈2.5% unmapped). We intersected DMC windows with the union of hippocampal DARs across 6 h, 12 h and 24 h using BEDTools intersect. Overlap was defined as any base-pair intersection (≥1 bp); a sensitivity check required ≥20% reciprocal overlap. Sequences for overlapping loci were extracted from mm10 with BEDTools getfasta. To provide a broader context, we also performed a global DAR analysis, where we extracted sequences for the union of all hippocampal DARs (mm10) and scanned them directly. For both analyses, motif finding used FIMO (MEME Suite) against the JASPAR CORE vertebrate non-redundant library (2024 release; MEME format). Background nucleotide frequencies were estimated from the target sequences with fasta-get-markov (order 1). Matches with q < 1×10^{-4} were retained.

3. Results

3.1. Time course of gene expression of inflammatory markers in the long-term GWI mouse model

The relative abundance of six known inflammatory markers were measured in the HPC and CTX across the four treatment conditions, with *CORT + DFP + Saline* serving as the control. The results are shown in Fig. 2. Across genes, timepoint exerted a strong effect on expression (two-way ANOVA on the $\log_2$ scale): Ccl2 $F(3,24) = 97.48$, $p = 1.4 \times 10^{-13}$; Il1b $F(3,24) = 181.19$, $p = 1.3 \times 10^{-16}$; Il6 $F(3,24) = 10.34$, $p < 1 \times 10^{-4}$; Osm $F(3,24) = 27.17$, $p = 6.9 \times 10^{-8}$; Tnfa $F(3,24) = 72.60$, $p = 3.5 \times 10^{-12}$. Brain region and Brain region × Timepoint were not significant, and no HPC–CTX simple contrast survived FDR at any timepoint (all FDR-adjusted $p \geq 0.14$). Planned contrasts versus Control within each brain region (FDR adjusted) showed a rapid peak at 6 h, attenuation by 12 h, and gene-dependent recovery by 24 h. Tnfa, Il1b, and Ccl2 were elevated at 6 h, 12 h, and 24 h in both regions (all FDR-adjusted $p < 0.001$ at 6–12 h; 24 h remained significant for each marker: e.g., Tnfa 24 h—HPC $p = 5.0 \times 10^{-5}$, CTX $p = 4.4 \times 10^{-6}$; Il1b 24 h—HPC $p = 1.2 \times 10^{-7}$, CTX $p = 8.7 \times 10^{-10}$; Ccl2 24 h—HPC $p = 3.1 \times 10^{-7}$, CTX $p = 5.2 \times 10^{-8}$). In contrast, Il6 was transiently elevated at 6 h and indistinguishable from control by 12–24 h (HPC 6 h 3.5 × [2.1–5.8], $p = 0.003$; HPC 24 h 0.8 × [0.5–1.3], $p = 0.577$; CTX 6 h $p = 0.013$; CTX 12 h $p = 0.830$; CTX 24 h $p = 0.725$). Osm transcript abundance increased at 6–12 h in both regions, then returned to baseline in HPC but not CTX by 24 h (HPC 24 h 1.8 × [1.2–2.8], $p = 0.051$; CTX 24 h 2.5 × [1.7–3.8], $p = 0.004$).

3.2. Differential gene expression by RNA-seq

In the HPC, RNA-seq analysis identified 701, 1,675, and 1757 unique genes that were differentially expressed at 6, 12, and 24 h, respectively, following the LPS injection compared to the control group (Fig. 3a; Supplementary Table 1). Notably, there were 474 unique genes differentially expressed in common across all the time points. This constitutes approximately 27% (474 out of 1758) of the differentially expressed genes at 24 h after LPS. All 474 genes exhibited a consistent direction of change; 303 increased and 171 decreased in transcript abundance across time. No gene that was significant at all three time points reversed direction.

Similarly, in the CTX, RNA-seq analysis identified 1,453, 1,937, and 1556 unique genes that were differentially expressed 6, 12, and 24 h following the LPS injection, respectively, compared to the control group (Fig. 3b; Supplementary Table 2). There were 649 unique genes differentially expressed across all the time points, with 366 showing increased and 283 decreased transcript abundance, which is approximately 42%

(649 out of 1556) of the differentially expressed genes at 24 h after LPS. No genes reversed direction. The directionality of genes across at least two timepoints for HPC and CTX are provided in Supplementary Table 1 for HPC and Supplementary Table 2 for CTX).

Gene pathway analysis of the 474 differentially expressed genes in the HPC and a separate gene pathway analysis the 649 genes differentially expressed in the CTX revealed that similar gene pathways were enriched in both brain regions. Specifically, 15 out of the top 20 GO terms were the same (Fig. 3c), with 10 of these 20 GO terms related to immune/stress responses.

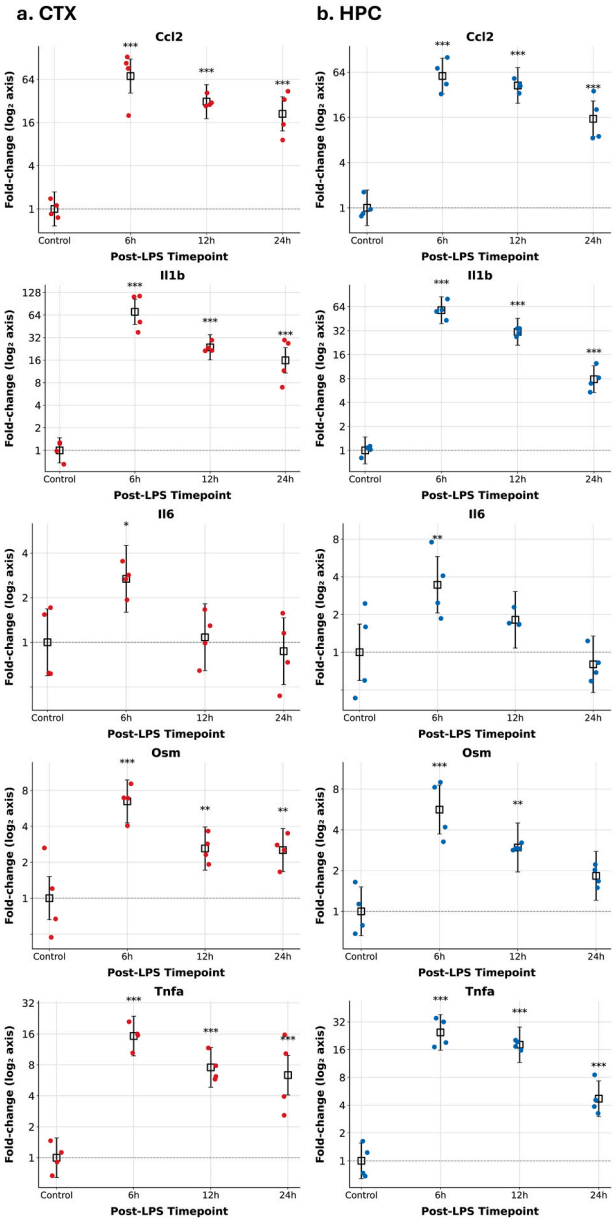

Fig. 2. Estimation plots of qPCR fold-change (vs. control, CORT–DFP) for five inflammatory genes at 6, 12, and 24 h post-LPS, shown separately for **a.** cortex (CTX) and **b.** hippocampus (HPC). Dots represent individual animals ($n = 4$ per cell). Hollow black squares with black error bars show model means (estimated marginal means from a two-way ANOVA on the $\log_2$ scale) and 95% CIs, back-transformed to the fold-change scale. The dashed line marks the control level (FC = 1). Because different animals were used at each timepoint, points are not connected. Asterisks above 6 h/12 h/24 h indicate BH–FDR–adjusted contrasts versus the control within the same brain area ($p < 0.05$, $*p < 0.01$, $**p < 0.001$).

3.3. Cell proportions analysis

To assess whether the transcriptional differences observed by RNA-seq (Fig. 3) could be explained by underlying changes in cellular composition, we next estimated relative cell-type proportions in hippocampus and cortex samples using a deconvolution approach. This analysis was necessary to determine whether observed expression differences reflected altered cell abundance (a potential confound in bulk tissue and multi-omics studies (Gong and Szustakowski, 2013);) or whether they more likely reflected transcriptional regulation within stable cell populations. The proportions of different cell types in the HPC and CTX were estimated from RNA-seq data at each time point: control, 6 h, 12 h, and 24 h post-LPS challenge. We estimated the proportions of neurons, astrocytes, oligodendrocyte precursor cells (OPCs), myelinating oligodendrocytes (MOs), microglia, and endothelial cells. The results are shown in Fig. 4.

Our findings revealed that, in the HPC, neurons comprised ~27% of the cell population (overall average across all timepoints), with astrocytes, OPCs, myelinating oligodendrocytes, microglia, and endothelial cells averaging ~12%, 19%, 25%, 6%, and 11%, respectively. In the CTX, neurons made up ~23% of the cell population, while astrocytes, OPCs, myelinating oligodendrocytes, microglia, and endothelial cells averaged ~10%, 17%, 34%, 6%, and 10%, respectively. Statistical tests on ILR-transformed proportions showed no significant evidence of time-dependent changes in overall composition in CTX (Wilks' $\lambda = 0.195$, $F(15, 19.7) = 1.06$, $p = 0.442$) or HPC (Wilks' $\lambda = 0.074$, $F(15, 19.7) = 2.06$, $p = 0.067$; Pillai's trace = 1.584, $F(15, 27) = 2.01$, $p = 0.055$). In addition, no individual cell type survived FDR correction in CLR-based tests, and sensitivity analysis using Dirichlet regression models providing the same result, with no significant time effects detected in either brain region. These findings indicate that transcriptional alterations following LPS are unlikely to be driven by major differences in cell composition, more likely reflecting regulatory alterations within cell types. On this basis, we next examined chromatin accessibility to determine how regulatory elements were dynamically altered by LPS exposure.

3.4. Chromatin accessibility

To identify regions of open chromatin accessible to transposase and indicative of regulatory activity, we performed ATAC-seq in the HPC and CTX. In the HPC, ATAC-seq analysis identified 15, 1,233, and 83 unique regions that were differentially accessible at 6, 12, and 24 h, respectively, following the LPS injection compared to the control group (Fig. 5a; Supplementary Table 3). Five (5) unique genes were consistently altered across all time points. All 5 genes (*Pax5, Sh2b2, Cdk8, Antxr1, Ush1c*) consistently had lower accessibility, and no gene that was significant at all three time points reversed direction. In the CTX, ATAC-seq analysis identified 183, 25, and 1860 unique regions that were differentially accessible at 6, 12, and 24 h, respectively, following the LPS injection compared to the control group (Fig. 5b; Supplementary Table 4). There were 15 unique genes associated with differentially accessible regions in common across all time points. Of these, 10 genes showed consistent directionality: 2 showed increased accessibility (*Itpr2, Snx1*) and 8 showed decreased accessibility (*Hhat, Gm29687, Acsbg2, Atp8b4, Aldob, Sh2b2, 1600010M07Rik, Txlng*). Five genes (*Cacna1e, Mir3084-2, Pappa, Ptprd, Galnt2*) were significant at all three time points but exhibited inconsistent accessibility, being decreased at 6 h and 12 h and increased at 24 h. The directionality of genes across at least two timepoints for HPC and CTX are provided in Supplementary Table 3 for HPC and Supplementary Table 4 for CTX).

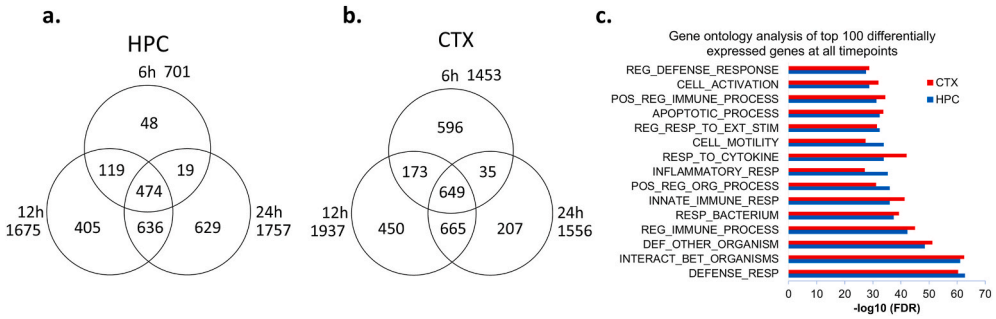

Fig. 3. Differentially expressed unique genes against control group, 6, 12, and 24 h after LPS (n = 3 for control groups, n = 4 for each LPS timepoint group). **a.** HPC. **b.** CTX. **c.** Gene ontology analysis of the genes differentially expressed in HPC (474 genes) and CTX (649 genes). Among the top 100 differentially expressed genes at all three time points, 15 of the top 20 GO terms are the same for HPC and CTX.

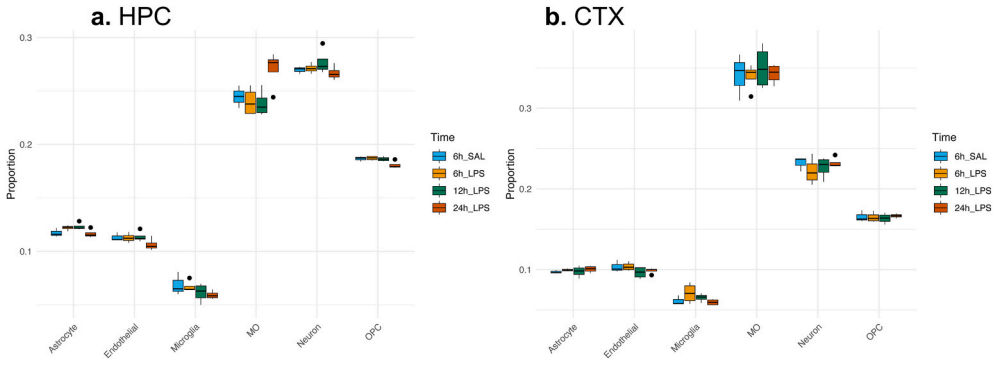

Fig. 4. Estimated cell proportions from RNA-seq data. **a.** HPC (left) and **b.** CTX (right) cell proportions estimated for five cell types of interest in control, 6, 12, and 24 h after LPS exposure conditions (median and quartiles for n = 3 for control groups, n = 4 for each LPS timepoint group). OPC: oligodendrocyte precursor cells. MO: myelinating oligodendrocytes. Cell-type composition appeared stable across time in both hippocampus and cortex.

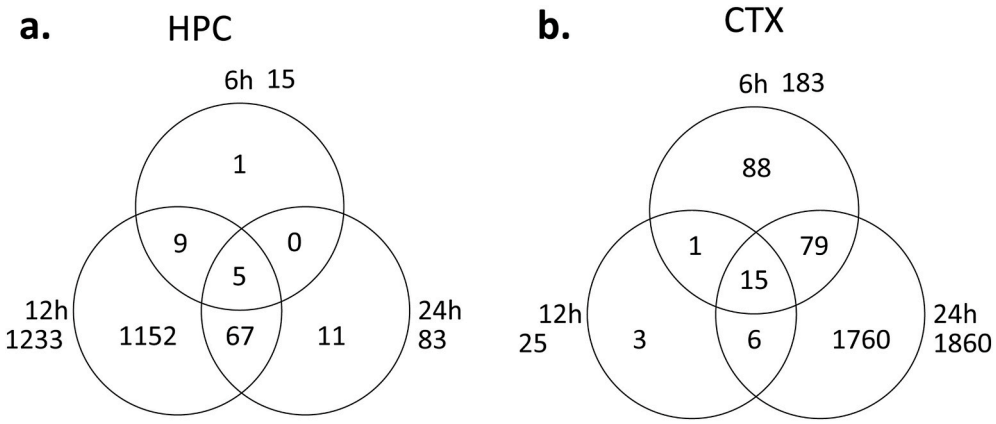

Fig. 5. Differential ATAC-seq peaks at each timepoint (6hr, 12hr, 24hr) against control group, after LPS exposure (n = 3 for control group, n = 4 for each LPS timepoint group) for **a.** HPC and **b.** CTX.

3.5. DNA methylation modifications in brain

To examine the reliability of the RRBS datasets, we performed pairwise comparisons of DNA methylation levels for each brain region. In initial analyses, all comparisons yielded correlation coefficients above 0.8, indicating strong reproducibility across samples (Supplementary Figs. 1 and 2 for HPC and CTX). We also found evidence for broad and consistent genomic coverage across time points by RRBS. In the HPC, the numbers of CpG sites analysed were 1,380,165, 1,296,182, and 1,164,178 for control vs 6 h, control vs 12 h, and control vs 24 h comparisons, respectively. In the CTX, the numbers of CpG sites analysed were 1,335,934, 1,376,872, and 1,370,712 for control vs 6 h, control vs 12 h, and control vs 24 h comparisons, respectively.

In the HPC, 3,011, 3,872, and 3905 genes were associated with differential methylation at 6, 12, and 24 h after LPS exposure, respectively (Fig. 6a; Supplementary Table 5). Of these 2101 genes were differentially methylated at all three time points, representing approximately 54% (2101 out of 3905) of the differentially methylated genes at 24 h after LPS. In contrast to the HPC, in the CTX there were 0, 15, and 1 gene(s) associated with differential methylation at these same time

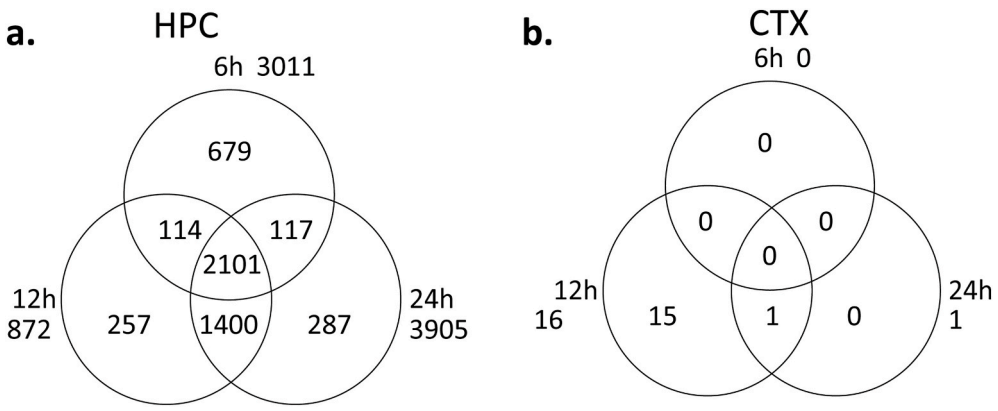

Fig. 6. Differentially methylated genes against control group, after LPS in **a.** HPC (n = 3 for control group, n = 4 for each LPS timepoint group) and **b.** CTX (n = 4 for all groups). DNA methylation modifications are largely confined to the HPC.

points (Fig. 6b; Supplementary Table 6). No genes in the CTX were differentially methylated across all three time points.

To evaluate the directionality of significant DNA methylation changes across timepoints, we analysed the data at both the gene level and the CpG level. At the gene level, we restricted the analysis to promoter-associated CpGs, to aid interpretability and because promoter methylation is most directly linked to transcriptional regulation (Jones, 2012). For each gene, CpGs were collapsed into a consensus call at each time point, and genes were classified as hyper- or hypomethylated only if all associated CpGs showed the same direction of change. Genes with mixed CpG directions at a time point were excluded. This conservative approach follows established methods to capture consistent promoter methylation changes while minimizing spurious assignments (Akalin et al., 2012; Jühling et al., 2016; Peters et al., 2015).

In the HPC across all 3 timepoints, 1824 genes had non-mixed calls across all three time points; of these, 1777 were consistently hypermethylated, 5 consistently hypomethylated, and 42 showed inconsistent directionality across timepoints. At the CpG level, each locus was evaluated independently. Of the 2029 significant CpGs across all three time points, 2025 CpGs were consistently hypermethylated and 4 consistently hypomethylated, with no inconsistent loci. The directionality of DNA methylation changes across at least two timepoints are provided in Supplementary Table 5 for HPC and Supplementary Table 6 for CTX**.** Together, the promoter-focused gene-level analysis and the CpG-level analysis indicate that the large majority of methylation changes that persist across all timepoints are directionally consistent.

For GO enrichment on DNA methylation-derived gene sets in the HPC, we used goseq with length-bias correction and a union-of-observed-genes background, applied to the top 100 genes present at all three time points and ranked by minimum q-value. Across 32 FDR-significant terms, the leading terms were neurogenesis, generation of neurons, neuron development, and regulation of cell differentiation/development, axon development and cell projection organisation. These results indicate that the sustained methylation signals converge on pathways governing neuronal differentiation, axonogenesis and related projections (see Supplementary Table 5 for the full term list and statistics).

When compared to differentially expressed genes, 40 unique genes were both differentially expressed and methylated at all time points compared to the control in the HPC. Among these genes, expression changes were directionally consistent (18 up-regulated, 22 down-regulated). Five genes were supported by multiple stable CpGs (four with two CpGs each and one, *Fgfr2*, with seven), all showing hypermethylation; the remainder were supported by a single stable CpG. Most stable CpGs mapped to promoter regions, with a minority in gene bodies. Promoter hypermethylation was most often associated with decreased transcript abundance, reflecting the expected inverse relationship, while a small subset exhibited concordant or context-dependent patterns (Supplementary Table 7). Functional enrichment analysis of these 40 genes showed over-representation of developmental and vascular processes, suggesting that integrated methylation and expression changes converge on pathways important for HPC structural regulation and plasticity (Supplementary Table 7).

In terms of correspondence between DARs and DMCs, of the 5 genes that showed DARs across all 3 timepoints (Fig. 5), one gene, *Pax5*, showed both significant DARs and DMCs in the HPC, but this gene did not show differential expression. Since no genes showed significant DMCs in the CTX (Fig. 6), there was no overlap between DARs and differential expression in the CTX. In addition, none of the 15 genes showing DARs at all 3 timepoints in the CTX (Fig. 5) overlapped with differentially expressed genes.

3.6. *Transcription factor binding site analysis using MEME suite*

To identify transcription factor binding targets in the HPC potentially affected by the exposures, we prioritized genes that exhibited coordinated changes in expression, chromatin accessibility, and DNA methylation. Sequences associated with DMCs were extended by ±50 bp to capture adjacent regulatory elements. In genomic regions containing DMCs, we found significant enrichment of transcription factors that are known to be activated by LPS exposure (Supplementary Table 8). Notably, NFKB1, a key component of the NF-κB complex, is a primary responder to LPS, playing a pivotal role in the inflammatory response, immune function, and cell survival (FDR p value < 0.05). CREB1, another significant transcription factor, is activated in response to stress and inflammatory signals, regulating genes crucial for cell survival, proliferation, and immune response (FDR p value < 0.05). Additionally, EGR1, which is rapidly induced by both LPS and stress, functions in the regulation of inflammation, cell growth, and apoptosis (FDR p value $<$ 0.01). The transcription factor c-JUN, part of the AP-1 complex, is also activated by these stimuli, influencing the expression of genes involved in cell proliferation, apoptosis, and inflammation. Finally, MYC, a well-known regulator, can be activated by stress and inflammatory signals, affecting cell cycle progression, apoptosis, and metabolism.

Intersecting HPC DMC windows (±50 bp) with the union of DARs revealed one overlapping locus, consistent across permissive (≥1 bp) and stricter (≥20% reciprocal) criteria. Motif scanning of this region identified binding sites for zinc-finger proteins (e.g., ZNF530, ZFP14), bHLH factors (ASCL1, MYOD1), and TCF/EBF family members, suggesting potential regulatory influence. A complementary global scan across all DARs (n = 1522) yielded abundant motifs, most notably ETS-like GGAA repeats, CTCF, RFX/SRF, and nuclear receptor motifs (e.g., RXR partners, PPAR, thyroid and retinoid receptors (Supplementary Table 9). Together, these analyses indicate that while direct overlap of

Table 1
Pathway analysis of genes differentially methylated and expressed at all timepoints in brain and differentially methylated in HPC and blood. Thirty-three (33) genes were differentially expressed in HPC and methylated in the HPC and in blood across all 3 timepoints.

Gene Set Name	# Genes in Gene Set (K)	# Genes in Overlap (k)	k/K	p-value	FDR q-value	-Log10(FDR)
GLIAL_CELL_DIFFERENTIATION	235	4	0.017	0.0000329	0.017	1.76955108
RESPONSE_TO_WOUNDING	578	5	0.0087	0.0000792	0.0279	1.5543958
GLIOGENESIS	320	4	0.0125	0.000109	0.035	1.45593196

Table 2
Seven genes associated with LPS exposure showing differential methylation in blood and differential methylation and expression in the HPC included in the GO pathway analysis, with functions in immune and glial responses.

Gene Name	Full Gene Name	Role in the CNS/neuroinflammatory/ glial function
FGFR2	Fibroblast Growth Factor Receptor 2	Plays a role in glial function, particularly in astroglial cells within the postnatal mouse brain.
PLPP3	Phospholipid Phosphatase 3	Has a notable role in glial function, especially in astroglial cells.
CDKN1A	Cyclin Dependent Kinase Inhibitor 1A	Plays a role in the acute response to inflammation within the CNS.
ITPK1	Inositol-Tetrakisphosphate 1-Kinase	Involved in inositol signalling pathways, crucial for various cellular processes.
CSPG5	Chondroitin Sulfate Proteoglycan 5	May function as a neural growth and differentiation factor.
STAT3	Signal Transducer and Activator of Transcription 3	Involved in microglial polarisation and modulation of microglia-dependent neuroinflammation.
SPINT1	Serine Peptidase Inhibitor, Kunitz Type 1	Associated with the positive regulation of glial cell differentiation.

DNA methylation and accessibility changes was limited, DARs broadly harbour transcription factor recognition sites relevant to chromatin regulation and cellular signalling.

3.7. DNA methylation modifications in blood

To examine the reliability of our approach, we performed pairwise comparisons of DNA methylation levels and found correlation coefficients greater than 0.8 for all comparisons, indicating high reproducibility in our dataset (Supplementary Figure 3). Consistent with samples from brain, we found evidence for broad and consistent genomic coverage across time points by RRBS in the blood samples. The numbers of CpG sites analysed were 1,201,496, 1,083,654, and 1,191,151 for control vs 6 h, control vs 12 h, and control vs 24 h comparisons, respectively.

There were 11,025, 11,321, and 11,275 unique genes associated with differential methylation 6 h, 12 h and 24 h after LPS exposure respectively, compared to the control condition (Supplementary Table 10). Of these 9244 genes were differentially methylated at all three time points representing approximately 82% (9244 out of 11,275) of the differentially methylated genes at 24 h after the LPS exposure, compared to the control condition.

Gene Ontology (GO) enrichment analysis of the top 100 genes consistently differentially methylated in blood across all three post-LPS time points revealed a strong convergence on immune- and stress-related pathways (Supplementary Table 10). The leading biological processes included regulation of immune system process, cytokine-mediated signalling, and leukocyte activation, alongside pathways related to cell differentiation and the cellular response to stress. These findings indicate that the large-scale DNA methylation changes observed in blood preferentially target genes involved in immune regulation and inflammatory signalling, consistent with the systemic immune activation expected following endotoxin exposure.

When compared to the genes differentially methylated at all time points in the HPC, there were 1299 unique genes differentially methylated in both the HPC and blood. Among the 1299 genes, 33 genes that were differentially methylated in blood were also differentially expressed in the HPC across all time points. Gene pathway analysis showed that these 33 genes cluster into 28 pathways, 3 of which are related to inflammation: 4 out of the 33 genes are included in the Glial Cell Differentiation pathway, 5 are included in Response to Wounding, and 4 genes are involved in Gliogenesis (for all FDRs, p value < 0.05; Table 1; see Supplementary Table 11 for the full pathway list). Seven (7) genes in these pathways have known roles in inflammation and glial function, including *Fgfr2, Plpp3, Cdkn1a, Itpk1, Cspg5, Stat3,* and *Spint1* (Table 2; see Supplementary Table 12, for the full gene list). Notably, consistent hypermethylation within a CpG island in the promoter region of *Stat3* (Signal transducer and activator of transcription 3) was observed with LPS exposure in the HPC, while multiple DMCs in close proximity showed differential methylation across all 3 timepoints in blood (Fig. 7). Stat3 transcript abundance in the HPC was significantly increased at all post-LPS time points relative to control, as determined

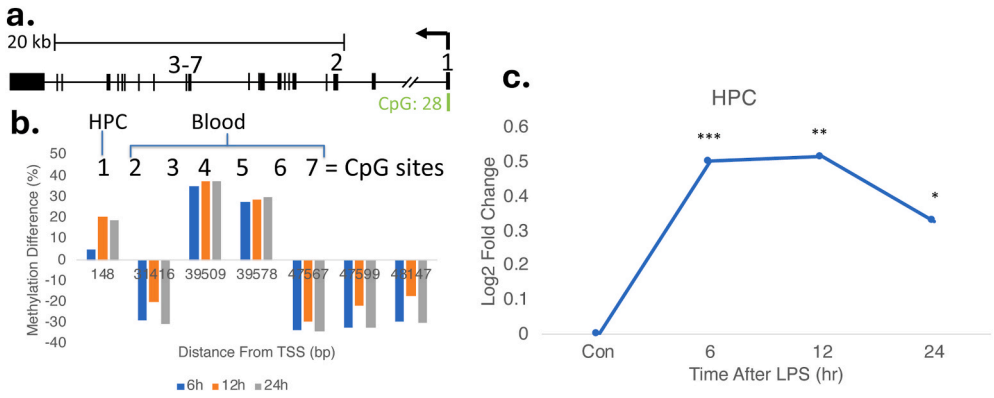

Fig. 7. Differential methylation and expression for the signal transducer and activator of transcription 3 (*Stat3*) gene. **a.** track for the *Stat3* gene, with numbers denoting approximate positions of DMCs relative to genic location. **b.** DMCs at each timepoint. **c.** Change in *Stat3* gene expression at each timepoint in the HPC, relative to control (n = 3 for control group, n = 4 for each LPS timepoint group). Differential expression was tested with DESeq2 (Wald test with Benjamini–Hochberg FDR correction). Asterisks denote significance after FDR adjustment (* = $q < 0.05$, ** = $q < 0.01$, *** = $q < 0.001$).

by DESeq2 (Wald test with Benjamini–Hochberg FDR correction).

4. Discussion

We find that prolonged CORT + DFP exposure leads to a primed neuroimmune state where robust transcriptional responses peak at 6 h post-LPS followed by partial resolution by 24 h, similar to the temporal pattern reported in acute exposure models (Locker et al., 2017; O'Callaghan et al., 2015). We observe persistent DNA methylation modifications in the HPC and in blood, providing evidence of cross-tissue concordance, whereas the CTX also showed strong transcription/chromatin changes but limited promotor-linked changes in DNA methylation.

Crucially, the multi-omic approach in the current study revealed enduring gene-co-regulation signatures that link brain and blood, providing evidence of epigenetic priming rather than transient LPS reactivity. We identified 33 genes showing both differential expression in HPC and persistent differential methylation in HPC *and* blood across all post-LPS time points. A number of these genes clustered in pathways related to immune regulation and glial cell function, biological effects implicated in other studies of GWI pathology. Our cell deconvolution analysis suggested that the proportions of major cell types in both the HPC and CTX remained relatively similar with LPS challenge, with only minor variations observed in oligodendrocytes and myelinating oligodendrocytes in the hippocampus. Notably, FGFR2 (Fibroblast Growth Factor Receptor 2), a gene essential in glial development and repair (Theophanous et al., 2024), showed enduring dysregulation in our model, consistent with previous reports of DFP and CORT effects on oligodendrocyte survival (Belgrad et al., 2019) and white-matter abnormalities reported in GWI veterans (Chao et al., 2015; Rayhan et al., 2013). Given stable cell-type composition by deconvolution, adequate RRBS assay power, and conservative, promoter-centred thresholds ($\geq$10 $\times$ coverage, $\Delta\beta \geq 5\%$, FDR <0.05), the limited CTX DMC signature may reflect smaller-magnitude or distal methylation changes at these acute time points, consistent with the robust CTX transcriptional and chromatin-accessibility responses we observed.

Our group previously reported that CORT + DFP exposure increases phosphorylated STAT3 in the brain, implicating it as a "neuroinflammation signal transducer" in an acute model (Locker et al., 2017). In the present study, we found evidence for sustained *Stat3* transcript upregulation after LPS challenge, and consistent hypermethylation in a CpG island of the *Stat3* promoter in HPC (with corresponding methylation changes in blood) across all time points. This novel epigenetic finding suggests that the initial neuroimmune insult may lead to a persistent regulatory change at the *Stat3* locus, potentially resulting in heightened inflammatory responsiveness and/or contributing to chronic glial priming. This idea is supported by our transcription factor binding analysis, which showed significant enrichment of consensus sites for NF-κB, AP-1 (c-JUN), CREB, EGR1, and other stress- or LPS-responsive factors in regions of differential methylation. These transcription factors drive acute gene expression in response to stress and infection and can also recruit chromatin modifiers that establish lasting epigenetic marks.

Our motif enrichment analyses also highlighted other regulators of potential relevance in both the DNA methylation TFBS scan (Supplementary Table 8) and the global DAR scan (Supplementary Table 9) including CTCF, a chromatin architectural protein whose binding is tightly modulated by DNA methylation (Ong and Corces, 2014; Phillips and Corces, 2009). These findings raise the possibility that altered chromatin looping and enhancer–promoter interactions mediated by CTCF could contribute to the transcriptional dysregulation observed in the HPC.

The relatively transient nature of chromatin accessibility changes we observed (from ATAC-seq) with few regions showing increased accessibility at later time points suggests that DNA methylation might serve as a stable modification of past neuroinflammatory events, whereas open chromatin states appear quickly reversible once the acute insult passes. Consistent with this view, our multi-omic comparison revealed minimal overlap between genes with persistent ATAC-seq changes and those showing coordinated expression and methylation changes at all timepoints. In the HPC, only one gene (Pax5) overlapped between ATAC-seq and methylation datasets, and no genes overlapped across all three modalities. Similarly, no overlap was observed in the cortex across RNA-seq, ATAC-seq, and methylation. These findings suggest that chromatin accessibility changes largely reflect transient, short-lived dynamics following LPS, whereas DNA methylation captures more enduring epigenetic regulation linked to sustained transcriptional outcomes. In this way, our prolonged exposure paradigm may capture both the immediate inflammatory wave and the longer-term epigenetic adaptations that follow.

The fact that we detected parallel DNA methylation changes in blood and brain for inflammation-related genes (e.g. *Stat3, Itpk1, Plpp3*) raises the possibility of blood-based epigenetic biomarkers for GWI. Indeed, a human study found widespread DNA methylation differences in peripheral blood mononuclear cells of GWI veterans compared to controls, notably ~10,767 CpG sites were differentially methylated (88% hypermethylated) in GWI, with over-representation of genes involved in metabolism and immune function (Trivedi et al., 2019). This concordance between animal and human data suggests that certain epigenetic signatures (for example, hypermethylation at immune gene promoters) could be a defining feature of GWI. Relatedly, a recent PET imaging study using a TSPO tracer reported elevated signals in the brains of GWI patients, consistent with enduring glial reactivity (microglia/astrocytes) and neuroinflammation (Alshelh et al., 2020). Such findings validate the central role of neuroimmune dysregulation long after the initial exposures. It is possible that latent epigenetic alterations in genes including *Stat3* and glial regulators, as observed in this study, could underlie chronic effects of GWI, though this remains to be tested.

A limitation of the current approach involves the use of a CORT + DFP + Saline group as the control condition; consequently, circadian or injection-related influences on gene expression over time cannot be completely excluded. However, because all animals shared identical exposure histories, handling, and injection procedures, non-specific stress effects are unlikely to account for the robust immune- and glia-related changes observed. In future studies, mechanistic interventions and paired blood transcriptomics with DNA methylation will help confirm causal pathways and refine peripheral biomarkers of the primed state. Finally, while the current study used only male mice (Ashbrook et al., 2018; Michalovicz et al., 2021; O'Callaghan et al., 2015), as the majority of veterans deployed during the 1990-91 Gulf War were male (~93%) (Brown et al., 2019), studies building upon recent investigations into the impact of Gulf War-relevant exposures in females are also needed (Alshelh et al., 2020; Heboyan et al., 2019; Krengel et al., 2021, 2024).

5. Conclusions

In summary, this study builds upon the work of our group and others by demonstrating how a prolonged exposure paradigm leads to integrated transcriptomic and epigenetic changes that were not evident in shorter-term exposure models. We corroborate that neuroinflammatory pathways (e.g. cytokine–STAT3 signaling) are acutely upregulated in GWI-like conditions (Locker et al., 2017), and further show that genes involved in glial function and differentiation (such as *FGFR2, CSPG5*) also undergo lasting changes, potentially contributing to white matter and cognitive deficits, as reported in veterans with GWI (Chao et al., 2015; Rayhan et al., 2013). The involvement of transcription factors including NF-κB, AP-1, and STAT3 in our methylation data suggests a mechanism of transcription factor-mediated epigenetic regulation, wherein an initial "priming" event instills long-term changes in the inflammatory set-point of the brain. These findings link acute neuroimmune responses to chronic dysregulation via epigenetic

modifications. Future studies can leverage this knowledge to explore targeted interventions, for example, to block key inflammatory transcription factors or modulate epigenetic enzymes to reverse the entrenched neuroinflammatory state. Ultimately, evidence indicating that GWI is a condition of persistent immunological maladaptation sustained by glial-centred and epigenetic mechanisms may aid in moving the field closer to addressing the root causes of GWI's enduring symptoms, beyond symptomatic relief, and toward therapies that can recalibrate the dysregulated neuroimmune network.

CRediT authorship contribution statement

A. Sasaki: Writing – review & editing, Writing – original draft, Visualization, Project administration, Methodology, Investigation, Formal analysis. **K.A. Kelly:** Writing – review & editing, Investigation, Funding acquisition, Formal analysis. **L.T. Michalovicz:** Writing – review & editing, Supervision, Project administration, Investigation, Funding acquisition, Formal analysis, Conceptualization. **D.G. Ashbrook:** Writing – review & editing, Investigation, Formal analysis. **S. Wijenayake:** Writing – review & editing, Investigation, Formal analysis. **J.P. O'Callaghan:** Writing – review & editing, Supervision, Resources, Funding acquisition, Conceptualization. **P.O. McGowan:** Writing – review & editing, Writing – original draft, Supervision, Resources, Project administration, Funding acquisition, Conceptualization.

Declaration of competing interest

The authors declare that they have no known competing financial interests or personal relationships that could have appeared to influence the work reported in this paper.

Acknowledgements

This work was supported by a CDMRP GWIRP research award and intramural funds from the CDC, National Institute for Occupational Safety and Health. The findings and conclusions in this report are those of the authors and do not necessarily represent the official position of the National Institute for Occupational Safety and Health, Centers for Disease Control and Prevention. This work was supported by the Assistant Secretary of Defense for Health Affairs through the Gulf War Illness Research Program. Opinions, interpretations, conclusions, and recommendations are those of the author and are not necessarily endorsed by the Department of Defense.

Appendix A. Supplementary data

Supplementary data to this article can be found online at https://doi.org/10.1016/j.bbih.2026.101207.

Data availability

ATAC-seq, RNA-seq, and RRBS datasets generated in this study have been deposited in the NCBI Gene Expression Omnibus (GEO) under accession numbers GSE325684, GSE325692, and GSE325694, respectively.

References

Akalin, A., Kormaksson, M., Li, S., Garrett-Bakelman, F.E., Figueroa, M.E., Melnick, A., Mason, C.E., 2012. methylKit: a comprehensive R package for the analysis of genome-wide DNA methylation profiles. Genome Biol. 13, R87. https://doi.org/10.1186/gb-2012-13-10-r87.

Alshelh, Z., Albrecht, D.S., Bergan, C., Akeju, O., Clauw, D.J., Conboy, L., Edwards, R.R., Kim, M., Lee, Y.C., Protsenko, E., Napadow, V., Sullivan, K., Loggia, M.L., 2020. In-vivo imaging of neuroinflammation in veterans with Gulf War illness. Brain Behav. Immun. 87, 498–507. https://doi.org/10.1016/j.bbi.2020.01.020.

Ashbrook, D.G., Hing, B., Michalovicz, L.T., Kelly, K.A., Miller, J.V., de Vega, W.C., Miller, D.B., Broderick, G., O'Callaghan, J.P., McGowan, P.O., 2018. Epigenetic impacts of stress priming of the neuroinflammatory response to sarin surrogate in mice: a model of Gulf War illness. J. Neuroinflammation 15, 86. https://doi.org/10.1186/s12974-018-1113-9.

Bailey, T.L., Johnson, J., Grant, C.E., Noble, W.S., 2015. The MEME suite. Nucleic Acids Res. 43, W39–W49. https://doi.org/10.1093/nar/gkv416.

Belgrad, J., Dutta, D.J., Bromley-Coolidge, S., Kelly, K.A., Michalovicz, L.T., Sullivan, K. A., O'Callaghan, J.P., Fields, RichardD., 2019. Oligodendrocyte involvement in Gulf War Illness. Glia 67, 2107–2124. https://doi.org/10.1002/glia.23668.

Benjamini, Y., Hochberg, Y., 1995. Controlling the false discovery rate - a practical and powerful approach to multiple testing. J. Royal Statistical Soc. Ser.B-Methodol. 57, 289–300.

Brown, M.C., Sims, K.J., Gifford, E.J., Goldstein, K.M., Johnson, M.R., Williams, C.D., Provenzale, D., 2019. Gender-based differences among 1990–1991 gulf war era veterans: demographics, lifestyle behaviors, and health conditions. Womens Health Issues 29, S47–S55.

Chao, L.L., Zhang, Y., Buckley, S., 2015. Effects of low-level sarin and cyclosarin exposure on white matter integrity in Gulf War Veterans. Neurotoxicology 48, 239–248. https://doi.org/10.1016/j.neuro.2015.04.005.

Cheng, C.-H., Guan, Y., Chiplunkar, V.P., Mortazavi, F., Medalla, M.L., Sullivan, K., O'Callaghan, J.P., Koo, B.-B., Kelly, K.A., Michalovicz, L.T., 2024. Nerve agent exposure and physiological stress alter brain microstructure and immune profiles after inflammatory challenge in a long-term rat model of Gulf War Illness. Brain, Behav.Immunity - Health 42, 100878. https://doi.org/10.1016/j.bbih.2024.100878.

Corces, M.R., Trevino, A.E., Hamilton, E.G., Greenside, P.G., Sinnott-Armstrong, N.A., Vesuna, S., Satpathy, A.T., Rubin, A.J., Montine, K.S., Wu, B., Kathiria, A., Cho, S.W., Mumbach, M.R., Carter, A.C., Kasowski, M., Orloff, L.A., Risca, V.I., Kundaje, A., Khavari, P.A., Montine, T.J., Greenleaf, W.J., Chang, H.Y., 2017. An improved ATAC-seq protocol reduces background and enables interrogation of frozen tissues. Nat. Methods 14, 959–962. https://doi.org/10.1038/nmeth.4396.

Dantzer, R., O'Connor, J.C., Freund, G.G., Johnson, R.W., Kelley, K.W., 2008. From inflammation to sickness and depression: when the immune system subjugates the brain. Nat. Rev. Neurosci. 9, 46–56. https://doi.org/10.1038/nrn2297.

Dobin, A., Davis, C.A., Schlesinger, F., Drenkow, J., Zaleski, C., Jha, S., Batut, P., Chaisson, M., Gingeras, T.R., 2013. STAR: ultrafast universal RNA-seq aligner. Bioinformatics (Oxford, England) 29, 15–21. https://doi.org/10.1093/bioinformatics/bts635.

Dolzhenko, E., Smith, A.D., 2014. Using beta-binomial regression for high-precision differential methylation analysis in multifactor whole-genome bisulfite sequencing experiments. BMC Bioinf. 15, 215. https://doi.org/10.1186/1471-2105-15-215.

Fornes, O., Castro-Mondragon, J.A., Khan, A., van der Lee, R., Zhang, X., Richmond, P.A., Modi, B.P., Correard, S., Gheorghe, M., Baranašić, D., Santana-Garcia, W., Tan, G., Chèneby, J., Ballester, B., Parcy, F., Sandelin, A., Lenhard, B., Wasserman, W.W., Mathelier, A., 2020. Jaspar 2020: update of the open-access database of transcription factor binding profiles. Nucleic Acids Res. 48, D87–D92. https://doi.org/10.1093/nar/gkz1001.

Franklin, K.B., Paxinos, G., 2013. Paxinos and Franklin's the Mouse Brain in Stereotaxic Coordinates.

Gong, T., Szustakowski, J.D., 2013. DeconRNASeq: a statistical framework for deconvolution of heterogeneous tissue samples based on mRNA-Seq data. Bioinformatics (Oxford, England) 29, 1083–1085. https://doi.org/10.1093/bioinformatics/btt090.

Haley, R.W., Kramer, G., Xiao, J., Dever, J.A., Teiber, J.F., 2022. Evaluation of a gene–environment interaction of PON1 and low-level nerve agent exposure with Gulf War illness: a prevalence case–control study drawn from the US Military Health Survey's national population sample. Environ. Health Perspect. 130, 057001.

Heboyan, V., Krengel, M.H., Sullivan, K., Iobst, S., Klimas, N., Wilson, C., Coughlin, S.S., 2019. Sex differences in gulf war illness: a reanalysis of data from the CDC air force study using CDC and modified kansas case definitions. J. Occup. Environ. Med. 61, 610–616.

Jones, P.A., 2012. Functions of DNA methylation: islands, start sites, gene bodies and beyond. Nat. Rev. Genet. 13, 484–492.

Jühling, F., Kretzmer, H., Bernhart, S.H., Otto, C., Stadler, P.F., Hoffmann, S., 2016. Metilene: fast and sensitive calling of differentially methylated regions from bisulfite sequencing data. Genome Res. 26, 256–262.

Kelly, K.A., Michalovicz, L.T., Miller, J.V., Castranova, V., Miller, D.B., O'Callaghan, J.P., 2018. Prior exposure to corticosterone markedly enhances and prolongs the neuroinflammatory response to systemic challenge with LPS. PLoS One 13, e0190546. https://doi.org/10.1371/journal.pone.0190546.

Koo, B.-B., Michalovicz, L.T., Calderazzo, S., Kelly, K.A., Sullivan, K., Killiany, R.J., O'Callaghan, J.P., 2017. Corticosterone potentiates DFP-induced neuroinflammation and affects high-order diffusion imaging in a rat model of Gulf War Illness. Brain Behav. Immun. https://doi.org/10.1016/j.bbi.2017.08.003.

Krengel, M., Keating, D., Chao, L., Dugas, J., Koo, B., Heeren, T., Quinn, E., Toomey, R., Steele, L., Klimas, N., 2024. Characterizing 1991 Gulf War women veterans from the Boston Biorepository and Integrative Network for Gulf War Illness: demographics, exposures, neuroimaging and cognitive outcomes. Clin. Neuropsychol. 38, 1454–1467.

Krengel, M., Sullivan, K., Heboyan, V., Zundel, C.G., Wilson, C.C., Klimas, N., Coughlin, S.S., 2021. Neurotoxicant exposures and rates of Chronic Multisymptom Illness and Kansas Gulf War Illness criteria in Gulf War deployed women veterans. Life Sci. 280, 119623.

Krueger, F., 2015. Trim Galore!: a Wrapper Around Cutadapt and Fastqc to Consistently Apply Adapter and Quality Trimming to Fastq Files, with Extra Functionality for RRBS Data. Babraham Institute.

Krueger, F., Andrews, S.R., 2011. Bismark: a flexible aligner and methylation caller for Bisulfite-Seq applications. Bioinformatics (Oxford, England) 27, 1571–1572. https://doi.org/10.1093/bioinformatics/btr167.

Langmead, B., Salzberg, S.L., 2012. Fast gapped-read alignment with Bowtie 2. Nat. Methods 9, 357–359. https://doi.org/10.1038/nmeth.1923.

Law, C.W., Chen, Y., Shi, W., Smyth, G.K., 2014. Voom: Precision weights unlock linear model analysis tools for RNA-seq read counts. Genome Biology 15 (2), R29. https://doi.org/10.1186/gb-2014-15-2-r29.

Livak, K.J., Schmittgen, T.D., 2001. Analysis of relative gene expression data using real-time quantitative PCR and the 2− ΔΔCT method. Methods 25, 402–408.

Locker, A.R., Michalovicz, L.T., Kelly, K.A., Miller, J., Miller, D.B., O'Callaghan, J.P., 2017. Corticosterone primes the neuroinflammatory response to Gulf War Illness-relevant organophosphates independently of acetylcholinesterase inhibition. J. Neurochem. 142, 444–455. https://doi.org/10.1111/jnc.14071.

Love, M.I., Huber, W., Anders, S., 2014. Moderated estimation of fold change and dispersion for RNA-seq data with DESeq2. Genome Biol. 15, 550. https://doi.org/10.1186/s13059-014-0550-8.

Lun, A.T.L., Smyth, G.K., 2016. Csaw: a Bioconductor package for differential binding analysis of ChIP-seq data using sliding windows. Nucleic Acids Res. 44, e45. https://doi.org/10.1093/nar/gkv1191.

Martin, M., 2011. Cutadapt removes adapter sequences from high-throughput sequencing reads. EMBnet J. 17, 10. https://doi.org/10.14806/ej.17.1.200.

Michalovicz, L.T., Kelly, K.A., Miller, D.B., Sullivan, K., O'Callaghan, J.P., 2021. The β-adrenergic receptor blocker and anti-inflammatory drug propranolol mitigates brain cytokine expression in a long-term model of Gulf War Illness. Life Sci. 285 (119962). https://doi.org/10.1016/j.lfs.2021.119962.

Mudge, J.M., Harrow, J., 2015. Creating reference gene annotation for the mouse C57BL6/J genome assembly. Mamm. Genome : Off. J.Int.Mammalian Genome Soc. 26, 366–378. https://doi.org/10.1007/s00335-015-9583-x.

O'Callaghan, J.P., Kelly, K.A., Locker, A.R., Miller, D.B., Lasley, S.M., 2015. Corticosterone primes the neuroinflammatory response to DFP in mice: potential animal model of Gulf War Illness. J. Neurochem. 133, 708–721. https://doi.org/10.1111/jnc.13088.

Ong, C.-T., Corces, V.G., 2014. CTCF: an architectural protein bridging genome topology and function. Nat. Rev. Genet. 15, 234–246.

Park, Y., Wu, H., 2016. Differential methylation analysis for BS-seq data under general experimental design. Bioinformatics 32, 1446–1453.

Passos, I.C., Vasconcelos-Moreno, M.P., Costa, L.G., Kunz, M., Brietzke, E., Quevedo, J., Salum, G., Magalhães, P.V., Kapczinski, F., Kauer-Sant'Anna, M., 2015. Inflammatory markers in post-traumatic stress disorder: a systematic review, meta-analysis, and meta-regression. Lancet Psychiatry 2, 1002–1012.

Peters, T.J., Buckley, M.J., Statham, A.L., Pidsley, R., Samaras, K., V Lord, R., Clark, S.J., Molloy, P.L., 2015. De novo identification of differentially methylated regions in the human genome. Epigenetics Chromatin 8, 6.

Phillips, J.E., Corces, V.G., 2009. CTCF: master weaver of the genome. Cell 137, 1194–1211.

Rayhan, R.U., Stevens, B.W., Timbol, C.R., Adewuyi, O., Walitt, B., VanMeter, J.W., Baraniuk, J.N., 2013. Increased brain white matter axial diffusivity associated with fatigue, pain and hyperalgesia in Gulf War illness. PLoS One 8, e58493. https://doi.org/10.1371/journal.pone.0058493.

Subramanian, A., Tamayo, P., Mootha, V.K., Mukherjee, S., Ebert, B.L., Gillette, M.A., Paulovich, A., Pomeroy, S.L., Golub, T.R., Lander, E.S., Mesirov, J.P., 2005. Gene set enrichment analysis: a knowledge-based approach for interpreting genome-wide expression profiles. Proc. Natl. Acad. Sci. U. S. A. 102, 15545–15550.

Sultana, E., Shastry, N., Kasarla, R., Hardy, J., Collado, F., Aenlle, K., Abreu, M., Sisson, E., Sullivan, K., Klimas, N., Craddock, T.J.A., 2024. Disentangling the effects of PTSD from Gulf War Illness in male veterans via a systems-wide analysis of immune cell, cytokine, and symptom measures. Milit. Med. Res. 11, 2. https://doi.org/10.1186/s40779-023-00505-4.

Theophanous, S., Sargiannidou, I., Kleopa, K.A., 2024. Glial cells as key regulators in neuroinflammatory mechanisms associated with multiple sclerosis. Int. J. Mol. Sci. 25, 9588. https://doi.org/10.3390/ijms25179588.

Trivedi, M.S., Abreu, M.M., Sarria, L., Rose, N., Ahmed, N., Beljanski, V., Fletcher, M.A., Klimas, N.G., Nathanson, L., 2019. Alterations in DNA methylation status associated with Gulf War illness. DNA Cell Biol. 38, 561–571. https://doi.org/10.1089/dna.2018.4469.

White, R.F., Steele, L., O'Callaghan, J.P., Sullivan, K., Binns, J.H., Golomb, B.A., Bloom, F.E., Bunker, J.A., Crawford, F., Graves, J.C., Hardie, A., Klimas, N., Knox, M., Meggs, W.J., Melling, J., Philbert, M.A., Grashow, R., 2016. Recent research on Gulf War illness and other health problems in veterans of the 1991 Gulf War: effects of toxicant exposures during deployment. Cortex; J. Devote Stud. Nervous Syst. Behav. 74, 449–475. https://doi.org/10.1016/j.cortex.2015.08.022.

Young, M.D., Wakefield, M.J., Smyth, G.K., Oshlack, A., 2010. Gene ontology analysis for RNA-seq: accounting for selection bias. Genome Biol. 11, R14.

Zhang, Y., Liu, T., Meyer, C.A., Eeckhoute, J., Johnson, D.S., Bernstein, B.E., Nusbaum, C., Myers, R.M., Brown, M., Li, W., Liu, X.S., 2008. Model-based analysis of ChIP-Seq (MACS). Genome Biol. 9, R137. https://doi.org/10.1186/gb-2008-9-9-r137.